01,07,08,13

Study of surface properties and melting point of rhodium at different pressures

© M.N. Magomedov

Institute for geothermal problems and renewable energy —
branch of the joint Institute of high temperatures of the Russian Academy of Sciences,
Makhachkala, Russia

E-mail: mahmag4@mail.ru

Received April 16, 2025
Revised July 9, 2025
Accepted July 11, 2025

An analytical method is proposed for calculating the lattice and surface properties of rhodium (Rh) at any (corresponding to the solid phase) values of temperature T and pressure P. Within the framework of this method, the parameters of the pairwise interatomic Mie–Lennard-Jones potential for Rh are determined in a self-consistent manner. The obtained potential parameters were tested by calculating the equation of state and baric dependences of the elastic modulus (B_T) and the thermal expansion coefficient. Using this analytical method, the surface properties of rhodium were studied for the first time: specific surface energy (σ) and derivatives of σ in temperature and pressure: $\sigma'(P)_T = (\partial\sigma/\partial P)_T$. Both baric dependences of these functions along three isotherms: 300, 1000, 2000 K, and temperature dependences along three isobars: 0, 50, 100 GPa were obtained. Estimates for the fragmentation point of rhodium at different temperatures are obtained. It is shown that the function $\sigma'(P)$ for rhodium depends linearly on the value of the pressure derivative of the elastic modulus $B'(P) = (\partial B_T/\partial P)_T$. The dependences of Poisson's ratio on pressure and temperature have been studied. The baric dependence of the Rh melting point is calculated. The influence of the electronic subsystem on the obtained dependencies is studied.

Keywords: rhodium, equation of state, elastic modulus, thermal expansion, surface energy, Debye temperature, Gröneisen parameter, melting point.

DOI: 10.61011/PSS.2025.08.62248.80-25

1. Introduction

Rhodium (Rh) is one of the six transition metal elements of the „platinum group" (rhutenium, rhodium, palladium, osmium, iridium, platinum), which have similar physical and chemical properties. Rhodium was discovered by the English scientist William Hyde Wollaston in 1803.Thanks to its corrosion resistance, high melting temperature (2236 K), low electrical resistance, high reflectivity, structural stability and catalytic properties, rhodium is widely applied in various fields of science and engineering. Unique properties of rhodium have been studied for a long time both experimentally and theoretically [1–13]. At the same time, due to difficulties of obtaining rhodium and removing impurities from it, some of its properties are either experimentally understudied or not studied at all. The rhodium properties were theoretically studied by methods of computer simulation as well. However, recently performed calculations both of the equations of state and baric dependences of the various properties of rhodium have shown contradictory results [9–14]. Some properties of rhodium are unstudied even theoretically. For example, the literature has no data about a dependence of a specific surface energy of rhodium on neither the temperature T nor the pressure P. At the same time, increasing use of rhodium in catalytic converters as well as in metalorganic chemistry requires detailed investigation of the surface properties of rhodium at the various $P-T$-conditions. At this, whereas the equation of state, an elastic modulus and thermal expansion of solid rhodium are recently studied in detail [8-13], but the baric dependence of the melting point ($T_m(P)$) for rhodium is understudied. Only one 1959's experimental study by H.M. Strong and F.P. Bundy [1] for investigating the dependence $T_m(P)$ of rhodium. Two theoretical studies for investigating the dependence $T_m(P)$ for rhodium have been recently performed: using the Full-Potential Linear Muffin-Tin Orbital (FM-LMTO) method of computer simulation in [9] and the statistical moment method (SMM) in [14]. In this regard, an analytical method (i.e. without computer simulation and artificial intelligence), which is presented in [15–17], was taken in the present study to calculate the equation of state of rhodium and the baric dependences of its lattice and surface properties from unified positions. The same method was also taken to study the baric dependence of the Rh melting point.

2. Calculation method

Our used analytical method of calculation of the single-component crystal was presented in detail in [15–17]. In order to describe pairwise interatomic interaction, this method uses a four-parameter Mie–Lennard-Jones potential,

which is expressed as follows:

$$\varphi(r) = \frac{D}{(b-a)}\left[a\left(\frac{r_0}{r}\right)^b - b\left(\frac{r_0}{r}\right)^a\right], \qquad (1)$$

where D and r_0 — the depth and the coordinate of the potential minimum, $b > a > 1$ — numerical parameters, r — the distance between atom centers.

Using the „only nearest-neighbor interaction" approximation and applying the Einstein crystal model for the oscillation spectrum, the following expressions were obtained for specific (per unit area) surface energy of the facet (100) of the macrocrystal (σ), its isochoric and isobaric derivatives with respect to the temperature and the derivative of σ with respect to the specific area in the Refs. [15,16]:

$$\sigma(k_\mathrm{n}, R, T) = -\frac{k_\mathrm{n} D R^2}{12\alpha^{2/3} r_0^2}\left[U(R) + 3H_\mathrm{w}(R, T)\right], \qquad (2)$$

$$\sigma'(T)_v = \left(\frac{\partial\sigma}{\partial T}\right)_v = -\frac{3k_\mathrm{B}R^2\gamma}{2\alpha^{2/3}(b+2)r_0^2} F_\mathrm{E}\left(\frac{\Theta_\mathrm{E}}{T}\right), \qquad (3)$$

$$\sigma'(T)_P = \left(\frac{\partial\sigma}{\partial T}\right)_P = \sigma'(T)_v + v\alpha_p\left(\frac{\partial\sigma}{\partial v}\right)_T$$

$$= \sigma'(T)_v - \frac{2}{3}\sigma\alpha_p\Delta_p, \qquad (4)$$

$$\Delta_p = -\left[\frac{\partial\ln(\sigma)}{\partial\ln(\Sigma)}\right]_T = -\frac{1}{2}\left[\frac{\partial\ln(\sigma)}{\partial\ln(c)}\right]_T = -\frac{3}{2}\left[\frac{\partial\ln(\sigma)}{\partial\ln(v/v_0)}\right]_T$$

$$= 1 + \frac{U'(R) - \left[q - \gamma t_y\left(\Theta_\mathrm{E}/T\right)\right]9H_\mathrm{w}(R, T)}{2\left[U(R) + 3H_\mathrm{w}(R, T)\right]}. \qquad (5)$$

Here, k_n — the first coordination number, $R = r_0/c$ — the relative linear density of the crystal, $c = (6k_\mathrm{p}\, v/\pi)^{1/3}$ — the distance between the nearest-atom centers, k_p — the structure packing index, $v = V/N$ — the specific volume, V and N — the volume and the number of the crystal atoms, $\alpha = \pi/(6k_\mathrm{p})$, $k_\mathrm{B} = 1.3807 \cdot 10^{-23}$ J/K — the Boltzmann constant, Θ_E — the Einstein temperature, which is related to the Debye temperature by the relationship [17,18] $\Theta = (4/3)\Theta_\mathrm{E}$, $\gamma = -(\partial\ln\Theta/\partial\ln v)_T$ and $q = (\partial\ln\gamma/\partial\ln v)_T$ — the first and second Gröneisen parameters, $\alpha_p = (\partial\ln v/\partial T)_P$ — the coefficient of thermal volume expansion, Σ — the area of the system surface,

$$U(R) = \frac{aR^b - bR^a}{b-a},$$

$$U'(R) = R\left[\frac{\partial U(R)}{\partial R}\right] = \frac{ab(R^b - R^a)}{b-a},$$

$$H_\mathrm{w}(R, T) = \frac{6\gamma}{(b+2)}\frac{k_\mathrm{B}\Theta_\mathrm{E}}{Dk_\mathrm{n}} E_\mathrm{w}\left(\frac{\Theta_\mathrm{E}}{T}\right),$$

$$E_\mathrm{w}(y) = 0.5 + \frac{1}{[\exp(y)-1]},\ F_\mathrm{E}(y) = \frac{y^2\exp(y)}{[\exp(y)-1]^2},$$

$$t_y(y) = 1 - \frac{2y\exp(y)}{[\exp(2y)-1]},\quad v_0 = \frac{\pi r_0^3}{6k_p}.$$

We can easily see that when $T \to 0$ K the functions of (3) and (4) tend to zero at any value of the density R, which complies with the third law of thermodynamics. The formulas for calculating the Debye temperature Θ and the Grüneisen parameters, equation of state $P(v, T)$, $c(P, T)$, the thermal expansion coefficient $\alpha_p(P, T)$ and other properties of the crystal within the framework of this method are described in our studies [15,16].

The obtained expressions (2)–(5) make it possible to calculate the dependence of the surface properties on the normalized volume $v/v_0 = (c/r_0)^3 = R^{-3}$ and the temperature for the single-component crystal with a given structure (i.e. for given values of k_n and k_p), if the parameters of the interatomic potential (1) are known. Note that the expressions (2)–(5) do not take into account either vacancies or self-diffusion of atoms, because, as shown in [19,20], their influence becomes negligible when the crystal is compressed. Here, as well as in [15,16,20], the contribution by the electron subsystem to the thermodynamic parameters is not taken into account, because the potential (1) describes the pairwise interaction of electrically neutral atoms. In addition, as shown in the Refs. [21–24],, the errors that arise in the lattice properties calculation due to exclusion of the electron subsystem from consideration are negligibly small. For example, as indicated in [21], for gold the contribution by the electron subsystem to the pressure is 0.01 and 0.5 GPa at 1000 and 5000 K, respectively. This contribution is much smaller than the error in pressure measurements at these temperatures.

In the Ref. [25] we have proposed a method for calculating the dependence $T_\mathrm{m}(P)$, in which the dependence $T_\mathrm{m}(P)$ is calculated by the formula

$$T_\mathrm{m}(P) = T_\mathrm{m}\left(P, T_\mathrm{m}(0)\right)\exp\Big[-\frac{b}{3}\alpha_p\left(P, T_\mathrm{m}(0)\right)$$

$$\times\left[T_\mathrm{m}\left(P, T_\mathrm{m}(0)\right) - T_\mathrm{m}(0)\right]\Big], \qquad (6)$$

where $T_\mathrm{m}(0)$ — the crystal melting point at $P = 0$, $\alpha_p\left(P, T_\mathrm{m}(0)\right)$ — the thermal expansion coefficient at the pressure P, which is calculated along the isotherm $T_\mathrm{m}(0)$,

$$T_\mathrm{m}\left(P, T_\mathrm{m}(0)\right) = T_\mathrm{m}(0)\left[\frac{c\left(P, T_\mathrm{m}(0)\right)\Theta\left(P, T_\mathrm{m}(0)\right)}{c\left(0, T_\mathrm{m}(0)\right)\Theta\left(0, T_\mathrm{m}(0)\right)}\right]^2$$

$$\times\frac{f_y\left(y_\mathrm{w}\left(P, T_\mathrm{m}(0)\right)\right)}{f_y\left(y_\mathrm{w}\left(0, T_\mathrm{m}(0)\right)\right)}. \qquad (7)$$

The function $f_y(y_\mathrm{w})$ appears in (7) due to taking into account quantum effects and is written as

$$f_y(y_\mathrm{w}) = \frac{2[1-\exp(-y_\mathrm{w})]}{y_\mathrm{w}[1+\exp(-y_\mathrm{w})]},\ y_\mathrm{w} = \frac{\Theta_\mathrm{E}}{T} = \frac{3\Theta}{4T}.$$

This method was tested in Ref. [25] when calculating the dependence $T_\mathrm{m}(P)$ for crystals of gold, platinum and niobium, and it showed good results.

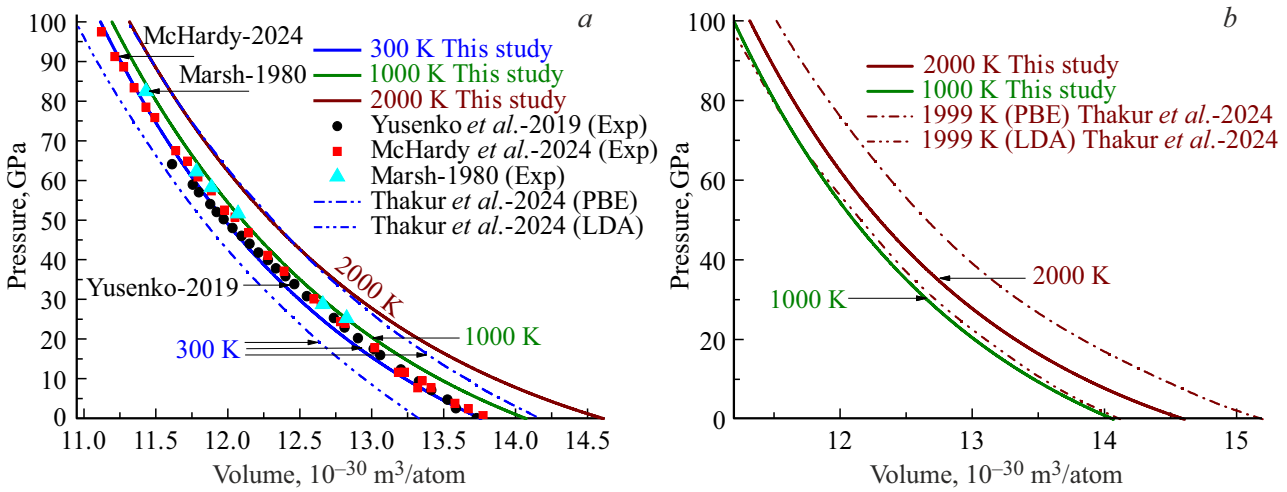


Figure 1. FCC-Rh equation of state. The solid lines mark our calculations at 300 (lower), 1000 (middle), 2000 K (upper). The dashdotted lines mark the calculations of the isotherms 301 (*a*) and 1999 K (*b*) from the Ref. [11]: with one dot for the PBE computer simulation method and with two dots for the LDA method. *a*) — The symbols mark the results of the experimental studies at 300 K: [2] — the solid triangles, [8] — the solid circles, [12] — the solid squares. *b*) Our calculations of the isotherms 1000 and 2000 K (the solid lines) and calculations of the isotherm 1999 K from [11]: the top is for PBE, and the bottom is for LDA.

3. Calculation results

3.1. Determination of the interatomic potential parameters

It is known that rhodium ($m(\mathrm{Rh}) = 102.906$ a.m.u.) has face-centered cubic (FCC) structure ($k_\mathrm{n} = 12$, $k_\mathrm{p} = 0.7405$) and does not experience polymorphous phase transitions up to 1000 GPa = 1 TPa [9]. The Rh melting point at $P = 0$ is $T_\mathrm{m}(P = 0) = 2236 \pm 3$ K [5]. The parameters of the pair interatomic potential (1) for FCC-Rh were initially determined by us with the use of a self-consistency method that is described in the Ref. [15]. At the same time, the values of r_0 and specific sublimation energy L_{00} were taken from the Ref. [26]. The index 00 means that this value is related to $P = 0$ and $T = 0$ K. By varying the values of Θ_{00} and γ_{00}, in the Ref. [15] we have determined the potential degrees b and a by fitting values of the thermal expansion coefficient α_p and the isothermal elastic modulus $B_T = -v(\partial P/\partial v)_T$ (that are calculated when $P = 0$ and $T = 300$ K) into the experimental data). However, the values of r_0, D, b and a, which are obtained in this way for FCC-Rh, did not allow obtaining a good dependence for the equation of state $P(v, T)$. Therefore, a new method of determination of the interatomic potential parameters (1) was used in the present study. The value of r_0 was corrected by taking into account the data from the study [5]: $c_{00} = 2.6851 \cdot 10^{-10}$ m is a distance between the nearest-atom centers when $P = 0$ and $T = 0$ K. The other three parameters (D, b, a) were determined by fitting the values of the thermal expansion coefficient α_p and the isothermal elastic modulusB_T, which are calculated when $P = 0$ and $T = 300$ K, into the experimental data. At the same time, we varied the following parameters: the specific sublimation energy (within the range $L_{00} = 500-700$ kJ/mol), the Debye temperature (within the range $\Theta_{00} = 200-700$ K) and the Grüneisen parameter (within the range $\gamma_{00} = 1-5$). These ranges are caused by inexactitude of the experimental estimates of the said parameters for FCC-Rh. For L_{00} it was indicated in the Refs. [26,27], so was for $\Theta_{00} = 480-530$ K in the Refs. [3,7,11,28] and so was for $\gamma_{00} = 0.8-2.8$ in the Refs. [1,7,11,28,29]. The new method of self-consistent determination of the parameters of the pair interatomic potential (1) is based on the fact that the values of L_{00}, Θ_{00} and γ_{00} are determined in the experiments with smaller accuracy than the values of α_p and B_T when $P = 0$ and $T = 300$ K. Therefore, the values of the potential parameters D, b and a were determined within the framework of formalism from [15,16] by fitting into the experimental values of α_p and B_T when $P = 0$ and $T = 300$ K. Thus, for FCC-Rh the following values of the parameters of the pair interatomic potential (1) were obtained:

$$r_0 = 2.681 \cdot 10^{-10}\,\mathrm{m}, \quad D/k_\mathrm{B} = 13\,800\,\mathrm{K},$$

$$b = 11.85, \quad a = 2.15. \tag{8}$$

Note that the parameters from (8) differ from the FCC-Rh parameters previously determined by us in the Ref. [15]. This is attributable to the fact that in the Ref. [15] the values of D, b and a were obtained when varying only the values of Θ_{00} and γ_{00} at the constant values $r_0 = 2.532 \cdot 10^{-10}$ m and $L_{00} = 555.76$ kJ/mol, which were taken from the Ref. [26].

In order to test the parameters of the interatomic potential from (8), the method from the Refs. [15,16] was taken to calculate the FCC-Rh properties. The first line of Figure 1

Table 1. FCC-Rh properties when $P = 0$ and $T = 300$ K. The first line is the calculation and further below are the data for FCC-Rh, which are known from the literature

$v = V/N$, Å^3/atom	α_p, 10^{-6} K^{-1}	B_T, GPa	$B'(P) = (\partial B_T/\partial P)_T$	Θ, K	γ
13.7555	29.244	225.541	6.693	311.532	2.303
13.757 [5] (13.7635) [6] 13.73 ± 0.07 [8] 13.766 ± 0.016 [10] (13.342(LDA)– 14.178(PBE)) [11] 13.764 ± 0.002, (13.764) [12] 13.762 ± 0.003 [13]	25.44 [5] (18.8(PBE)) [6] (25(PBE)–28(LDA)) [11] 20.5 ± 0.12, (29.9) [12] 33.6 ± 0.7 [13]	266.6 [3] 281 [4] (245.13–250.25) [6] 255–280 ± 160 [7] 301 ± 9 [8] 241.3 ± 0.65 [10] (245.3(PBE)– 305.6(LDA)) [11] 258 ± 3, (260.54) [12] 251(3) [13] (244.57(Vinet)– 251.08(BM)) [14]	3.1 ± 0.2, (2.9–4.6) [8] 5.34(24) [10] (5.2(LDA)–5.3(PBE)) [11] 5.36 ± 0.09, (5.114) [12] 5.7 ± 0.2 [13] (5.5(Vinet)– 5.07(BM)) [14]	489 [3] 350 [4] 480 [7] 490–530, (486.79(PBE)– 527.56(LDA)) [11] 1039 ± 7 [12] 350 [13]	2.29 [4] (0.8–2.8) [7] (2.3) [11]

shows the FCC-Rh properties that are calculated using the potential parameters from (8) when $P = 0$ and $T = 300$ K.

As can be seen in Table 1, the agreement between the calculated data and the experimental and theoretical (in brackets) estimates of the other authors is quite good. At the same time, it is necessary to take into account that the values of B_T and $B'(P) = (\partial B_T/\partial P)_T$ were experimentally determined not in the point $P = 0$, but within a certain pressure range [13]. The matter is that the value of B_T and $B'(P)$ are determined by fitting the experimentally-measured isothermal dependence $P(v)$ into three-parameter equations of state. The third-order Birch–Murnaghan equation is often used:

$$P(v) = \frac{3}{2} B_{0T} \left[\left(\frac{v}{v_0} \right)^{-7/3} - \left(\frac{v}{v_0} \right)^{-5/3} \right] \times \left\{ 1 - \frac{3}{4} (4 - B_0') \left[\left(\frac{v}{v_0} \right)^{-2/3} - 1 \right] \right\},$$

or the Vinet equation:

$$P(v) = 3B_{0T} \left(\frac{v}{v_0} \right)^{-2/3} \left[1 - \left(\frac{v}{v_0} \right)^{1/3} \right] \times \exp\left\{ 1.5(B_0' - 1) \left[1 - \left(\frac{v}{v_0} \right)^{1/3} \right] \right\}.$$

By fixing the value of v_0, the values of B_{0T} and B_0' are calculated within a certain pressure interval. I. e., these values are average for this interval. But if we take another equation for approximation or a somewhat different pressure interval, then the values B_T and B_0' are changed [13]. That is why when using the Birch–Murnaghan equation some values (BM) are obtained in the Ref. [14], while the other values are obtained therein when using the Vinet equations, as shown in Table 1. It is assumed in this calculation that the values of B_{0T} and B_0' are not changed within this pressure interval. In our calculations, the values of B_T and B' are calculated for the given temperature in the point $P = 0$. At the same time, in our case the values of B_T and B' are changed with increase of the pressure along the isotherm. Note that the value of Θ for rhodium is very approximately determined. It is indicated by a spread interval of the value of Θ for rhodium from other studies that are presented in Table 1. We have indicated incorrectness of modern experimental methods of determining the values of Θ and γ in the Ref. [28].

3.2. Equation of state

Figure 1 shows the isotherms of the FCC-Rh equation of state. The pressure is in GPa, while the specific volume is in Å^3/atom $= 10^{-30}$ m^3/atom. The studies [15,16] describe a method of calculating the equation of state $P(v, T)$ for a single-component crystal, whose atoms interact by the pair potential (1). The solid lines mark our calculations of the isotherms 300 (lower), 1000 (middle), 2000 K (upper). The dashdotted lines mark the results of calculations of the isotherms 301 (Figure 1, *a*) and 1999 K (Figure 1, *b*) from the Ref. [11]: with one dot for the PBE method (Perdew–Burke–Ernzerhof generalized gradient approximation) and with two dots for the LDA method (local density approximation). The symbols of the left graph mark the results of the experimental studies at 300 K: [2] — the solid triangles, [8] — the solid circles, [12] — the solid squares. Figure 1, *b* shows our calculations of the isotherms 1000 and 2000 K (the solid lines) and the calculations of the isotherm 1999 K from the Ref. [11] by the computer simulation methods: the upper line is for FBA and the lower line is for LDA. Note that in the Ref. [11] has also used a PBEsol calculation method, which is the PBE method modified for densely packed solids. The results of the PBEsol-method, which are obtained in the Ref. [11], lie between the dependences obtained by the PBE- and

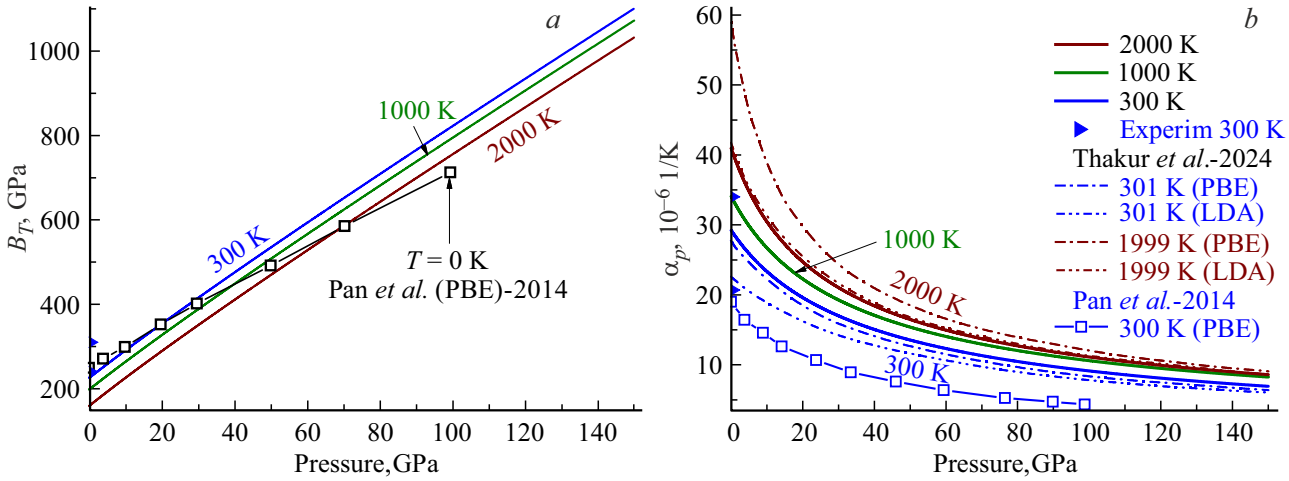


Figure 2. Baric dependence of *a*) the elastic modulus of FCC-Rh *b*) and its thermal expansion coefficient. The solid lines mark our calculations at 300, 1000, 2000 K, the dashdotted lines mark calculation of the isotherms 301 and 1999 K from the Ref. [11]: with one dot for the PBE method and with two dots for the LDA method. The symbols in the right axes show results of the experimental studies at 300 K and $P = 0$. The open squares show the calculations of the isotherm 0 K for B_T and the isotherm 300 K for α_p, which are obtained by the PBE method in the Ref. [6].

LDA-methods and, therefore, we did not include them in the graphs. As can be seen in Figure 1, the agreement between our calculations and the experimental data and the computer calculations of the other authors is quite good.

3.3. Elastic modulus and thermal expansion

Figure 2 shows the baric dependences of the isothermal elastic modulus (B_T is in GPa, Figure 2, *a*) and the isobaric thermal expansion coefficient (α_p is in 10^{-6} 1/K, Figure 2, *b*) for the FCC-Rh. Our studies [15,16] describe a method of calculating the functions $B_T(P, T)$ and $\alpha_p(P, T)$ for a single-component crystal, whose atoms interact by the pair potential (1). The solid lines mark our calculations of the isotherms 300, 1000, 2000 K. The opens squares show the calculations of the isotherm 0 K for B_T (Figure 2, *a*) and the isotherm 300 K for α_p (Figure 2, *b*), which are obtained by the PBE method in the Ref. [6]. The symbols in the right axes show a spread region of the experimental data at 300 K and when $P = 0$. The dashdotted lines of Figure 2, *b* mark the calculations of the isotherms 301 and 1999 K from the Ref. [11]: with one dot for the PBE computer simulation method (top) and two dots for the LDA computer simulation method (bottom). As can be seen in Figure 2, the agreement between our calculations and the experimental and computer calculations of the other authors is quite good. Therefore, we use this method with the interatomic potential parameters from (8) for predicting FCC-Rh properties, information about which is absent in the literature.

Figure 3 show the baric dependences of the derivatives of the isothermal elastic modulus with respect to the pressure ($B'(P) = (\partial B_T/\partial P)_T$, Figure 3, *a*) and the thermal expansion coefficient ($\alpha'_p(P) = (\partial \alpha_p/\partial P)_T$, in 10^{-6} 1/(GPa · K), Figure 3, *b*) along the isotherm 300 (the solid lines), 1000 (the dashed lines), 2000 K (the dotted lines). As we have not found any data about these dependences for FCC-Rh in the literature, it can be stated that we were the first to obtain these data. The estimates of other authors for $B'(P)$, which are obtained at 300 K and when $P = 0$, are shown in Table 1. Usually, these papers have experimentally determined the value of $B'(P)$ not in the point $P = 0$, but within the certain pressure range. At the same time, it was assumed in the majority of these studies that the value of $B'(P)$ was not changed with the pressure. However, as can be seen in Figure 3, the function $B'(P)$ decreases with increase of the pressure. It can be seen that the isotherms $B'(P)$ intersect each other in the point $P = 25$ GPa, $B'(P) = 6.13$. It indicates that at this pressure the function $B'(P)$ does not depend on the temperature.

3.4. Specific surface energy

Several different methods for calculating specific (per unit area) surface energy (σ) for a single-component substance crystal have been proposed to date (see, for example, [30–42]). But most of these methods (as, for example, in [32–36,38–42]) work only when $T = 0$ K and $P = 0$. Therefore, the issue of the dependence of the value of σ both on the temperature and the pressure at which the crystal is located is relevant. Table 2 shows the results of calculation of the FCC-Rh surface properties when $P = 0$ and when $T = 10$, 300, 1000, 2236 K, using the Eqs (2)–(5) and the potential parameters from (8).

The literature has a lot of estimates of the value of σ for the FCC-Rh facet (100). Below are some of them, which are obtained by authors using various methods of calculation:

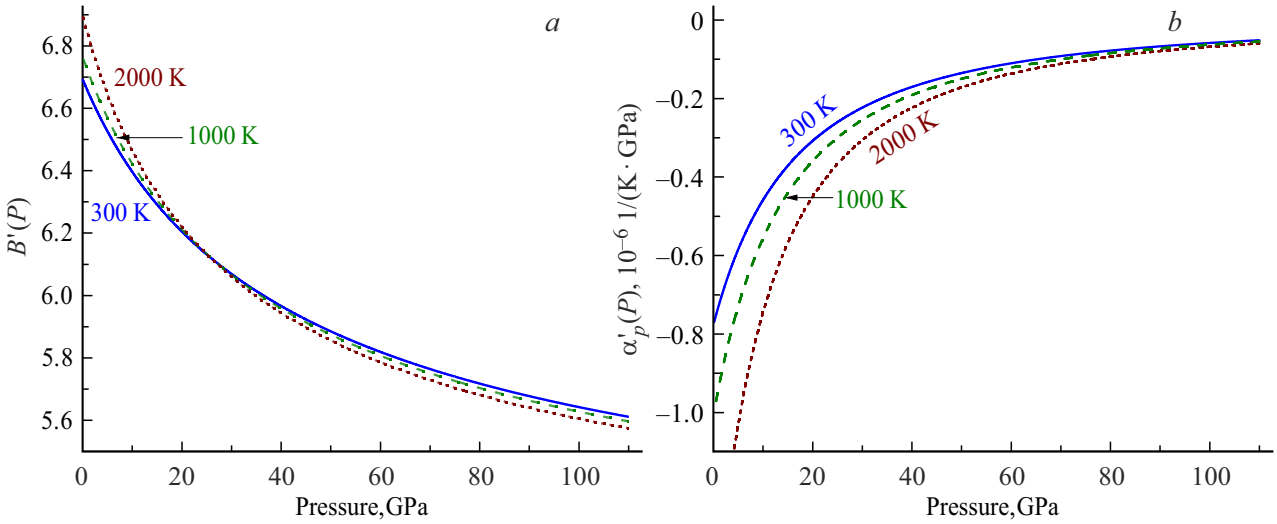


Figure 3. Baric dependences *a*) of the derivative of the isothermal elastic modulus with respect to the pressure and *b*) the derivative of the thermal expansion coefficient with respect to the pressure along the isotherms 300 (the solid lines), 1000 (the dashed lines), 2000 K (the dotted lines).

Table 2. Values of the FCC-Rh surface properties, which are calculated when $P = 0$ and at the four temperatures

T, K	v/v_0	$\sigma(100)$, 10^{-3} J/m^2	$-\sigma'(T)_v$,10^{-6} J/(m^{2}K)	$-\sigma'(T)_P$,10^{-6} J/(m^{2}K)	$\sigma'(P)_T$,10^{-3} J/(m^{2}GPa)	$\Delta_P = -(\partial \ln\sigma/\partial \ln\Sigma)_T$
10	1.00348	3324.99	$\sim 10^{-6}$	$\sim 10^{-6}$	9.51	1.0073
300	1.00951	3299.59	57.05	123.81	10.12	1.0377
1000	1.03238	3205.87	58.87	141.09	12.17	1.1278
2236	1.08238	3015.12	57.25	169.36	17.33	1.2945

$\sigma(100)$, 10^{-3} J/m^2 = 2490 (0 K) [30], 2325 (T_m) [31], 2810 [32], 3190 [33], 2190–2720 [34], 3120 [35], 3150 [36], 2600 [37], 3010 [38], 2470–3170 [39], 2350–3120 [40], 2560.307–3071.456 [42].

As can be seen, the agreement between our calculations and the estimates of the other authors is quite good. The estimates from the Refs. [30,31] were obtained by W.R. Tyson based on empirical relationships. But they are referred to as experimentally measured ones in studies of the other authors. In all other studies [32–42], the said estimates were obtained at 0 K. That is why there is no estimate of a value of the derivative $\sigma'(T)_P = (\partial\sigma/\partial T)_P$ for FCC-Rh in the literature. Using the estimates from the Refs. [30,31], one can obtain the value, which lies between our data for the isochoric and isobaric derivatives with respect to the temperature.

$$(\Delta\sigma/\Delta T)_{P=0} = -(2490-2325)/2236$$

$$= -73.8 \cdot 10^{-6}\,\text{J/(m}^2 \cdot \text{K)}.$$

But this is the value average across the interval 0–2236 K. As can be seen in Table 2, the function $\sigma'(T)_P$ nonlinearly decreases with the temperature from $\sigma'(0\,\text{K})_P = 0$ to $\sigma'(T_m)_P < 0$.

There is neither estimate of the value of $\sigma'(P) = (\partial\sigma/\partial P)_T$ in the literature; meanwhile, the dependence $\sigma(P)$ is necessary both when studying crack initiation under baric action on the crystal and for obtaining the equation of state for the nanocrystal. Note that the specific surface energy for FCC-Rh has never been experimentally estimated. The measurements are very labor-intensive and they can be carried out only in a region near the melting point of the crystal [43].

Figure 4, *a* shows the calculated baric dependences of the specific surface energy (in 10^{-3} J/m^2) for the FCC-Rh facet (100) along the isotherms (top-down) 300, 1000, 2000 K. It can be seen that at the certain pressure P_{max} the function $\sigma(P)$ reaches its maximum with the following coordinates:

$\sigma_{max} = 3519.8 \cdot 10^{-3}$ J/m^2 and $P_{max} = 64.4$ GPa for $T = 300$ K,

$\sigma_{max} = 3474.6 \cdot 10^{-3}$ J/m^2 and $P_{max} = 69.4$ GPa for $T = 1000$ K,

$\sigma_{max} = 3407.8 \cdot 10^{-3}$ J/m^2 and $P_{max} = 76.3$ GPa for $T = 2000$ K.

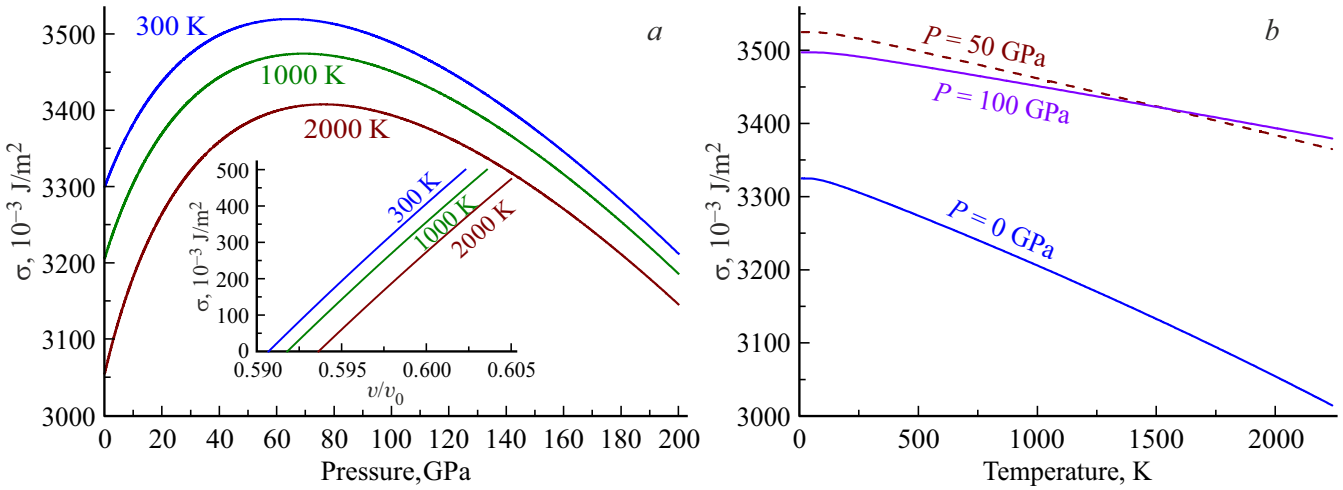


Figure 4. Dependences of the specific surface energy of the facet (100) for FCC-Rh on the pressure and the temperature. *a*) Baric dependences calculated along the isotherms 300, 1000, 2000 K. The insert has the dependence $\sigma(v/v_0, T)$ within a fragmentation area. *b*) Temperature dependences calculated along the isobars 0, 50 (the dashed line), 100 GPa.

Figure 4, *b* shows the calculated temperature dependences of the specific surface energy (in 10^{-3} J/m^2) for the FCC-Rh facet (100) along the isobars 100 and 50 GPa (the upper line), 0 GPa (the lower line). Intersection of the isobars 100 and 50 GPa is caused by a maximum in the function $\sigma(P)$, which is shown in the left graph. It can be seen in Figure 4 at certain compression $(v/v_0)_{\text{fr}} < 1$ (or when $P > P_{\text{fr}}$) the function $\sigma(v/v_0)$ transits into a negative region. The insert shows a dependence of the function $\sigma(v/v_0, T)$ within the fragmentation area. This behavior of the function $\sigma(v/v_0)$ when $v/v_0 < (v/v_0)_{\text{fr}}$ shall induce fragmentation of the crystal, where the crystal will tend to increase its specific (per atom) intercrystalline surface in any way. The effect of baric fragmentation was studied by us in more detail in the Ref. [44] on the example of crystals of neon, lithium and gold. For FCC-Rh, for the normalized volume $(v/v_0)_{\text{fr}}$ and pressure P_{fr} in a fragmentation point (where $\sigma = 0$) the following values are obtained:

$(v/v_0)_{\text{fr}} = 0.590674$ and $P_{\text{fr}} = 819.115$ GPa for $T = 300$ K,

$(v/v_0)_{\text{fr}} = 0.591815$ and $P_{\text{fr}} = 817.215$ GPa for $T = 1000$ K,

$(v/v_0)_{\text{fr}} = 0.593636$ and $P_{\text{fr}} = 814.683$ GPa for $T = 2000$ K.

3.5. Derivatives of the surface energy with respect to the temperature

Figure 5, *a* shows the calculated baric dependences of the derivative of the specific surface energy of the facet (100) with respect to the temperature (in 10^{-6} J/(m$^2 \cdot$ K)) along the isotherms (top-down) 300, 1000, 2000 K. The solid lines mark the isobaric derivative $\sigma'(T)_P$, while the dashed lines mark the isochoric derivative $\sigma'(T)_v$. It can be seen that at the low pressures (i.e., when $P < 50-70$ GPa) the inequality is fulfilled $|\sigma'(T)_P| > |\sigma'(T)_v|$. However, this inequality is reversed at the high pressures. Therefore, for the crystal, it is impossible to equate the isochoric and isobaric derivatives of the function σ with respect to the temperature, as is done in some studies.

Figure 5, *b* shows the calculated temperature dependences of the derivative of the specific surface energy with respect to the temperature ($\sigma'(T)_i = (\partial\sigma/\partial T)_i$, in 10^{-6} J/(m$^2 \cdot$ K), $i = v, P$) for FCC-Rh along the isobars 0, 50, 100 GPa. The solid lines mark the isobaric derivatives $\sigma'(T)_P$, while the dashed lines mark the isochoric derivatives $\sigma'(T)_v$. It can be seen from Figure 4 that with isobaric increase of the temperature, the value of σ decreases at any pressure. Therefore, in some studies, for the isobaric or isochoric temperature dependence of the specific surface energy a linear approximation of the following form was used:

$$\sigma(T) = \sigma(T = 0\,\text{K}) - \text{const}\,T. \tag{9}$$

However, as can be seen in Figure 5, the approximation (9) is valid only at the high temperatures and pressures. The use of the approximation (9) at the low temperatures can lead both to quantitative errors and to violation of the third law of thermodynamics. This is due to the fact that contribution by the surface to the specific (per atom) entropy and heat capacity (C_i, both isochoric — $i = v$, and isobaric — $i = P$) of the system is determined by the very function $\sigma'(T)_v$, i.e. the derivative of the specific surface energy with respect to the temperature [45]:

$$s_{\text{surf}} = -\left(\frac{\Sigma}{N}\right)\left(\frac{\partial\sigma}{\partial T}\right),$$

$$\left(\frac{C_i}{N}\right)_{\text{surf}} = T\left(\frac{\partial s_{\text{surf}}}{\partial T}\right)_{i,N} = -\left(\frac{\Sigma}{N}\right)T\left[\frac{\partial}{\partial T}\left(\frac{\partial\sigma}{\partial T}\right)_{v,N}\right]_{i,N}.$$

When $T = 0$ K, according to the third law of thermodynamics, for the specific entropy (s), heat capacity and

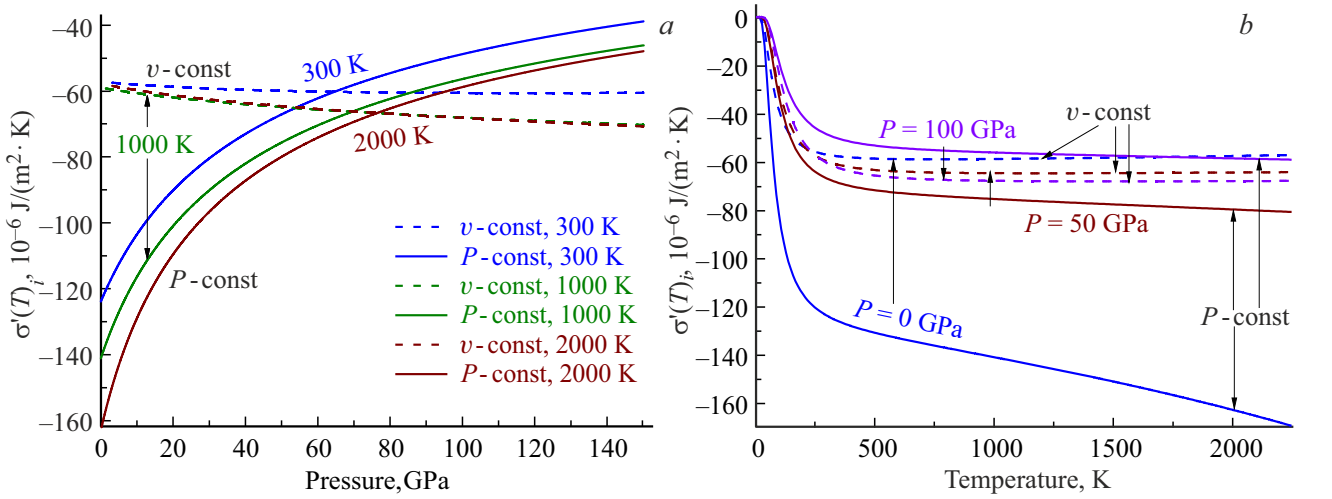


Figure 5. Dependences of the specific surface energy of the facet (100) with respect to the temperature for FCC-Rh on the pressure and the temperature. *a*) Baric dependences calculated along the isotherms 300, 1000, 2000 K. *b*) Temperature dependences calculated along the isobars 0, 50, 100 GPa. The solid lines mark the isobaric derivatives $\sigma'(T)_P$, while the dashed lines mark the isochoric derivatives $\sigma'(T)_\upsilon$.

function $\alpha_p \cdot B_T$ the following conditions must be satisfied:

$$\lim_{T\to 0\,\mathrm{K}} s = +0, \quad \lim_{T\to 0\,\mathrm{K}} \frac{C_i}{N} = +0,$$

$$\lim_{T\to 0\,\mathrm{K}} \alpha_p B_T = \lim_{T\to 0\,\mathrm{K}} \left(\frac{\partial s}{\partial \upsilon}\right)_T = +0.$$

In this regard, as shown in the paper [45], the function σ must satisfy the following conditions:

$$\left.\begin{aligned} &\lim_{T\to 0\,\mathrm{K}} \left(\frac{\partial \sigma}{\partial T}\right)_{i,N} = -0, \\ &\lim_{T\to 0\,\mathrm{K}} \left[\frac{\partial (\partial \sigma/\partial T)_{\upsilon,N}}{\partial \upsilon}\right]_{T,N} = -0, \\ &\lim_{T\to 0\,\mathrm{K}} T\left[\frac{\partial}{\partial T}\left(\frac{\partial \sigma}{\partial T}\right)_{\upsilon,N}\right]_{i,N} = -0. \end{aligned}\right\} \qquad (10)$$

The conditions (10) are valid for any crystal structure, at any specific volume of pressure as well as for any size and shape of the nanocrystal. Therefore, the use of the approximation (9) is not correct fro extrapolating the function $\sigma(T)$ to the low-temperature region.

3.6. Derivative of the surface energy with respect to the pressure

Figure 6 shows the calculated dependences of the derivative of the specific surface energy with respect to the pressure ($(\sigma'(P)_T = (\partial\sigma/\partial P)_T$, in $10^{-3}\,\mathrm{J/(m^2\cdot GPa)}$) for FCC-Rh. Figure 6, *a* shows the baric dependences calculated along the isotherms (from bottom to top) 300, 1000, 2000 K. Figure 6, *b* shows the temperature dependences calculated along the isobars (top-down) 0, 50, 100 GPa. It can be seen that when $P > 50$ GPa the function $\sigma'(P)_T$ varies linearly along the isobar with increase of the temperature. The inserts show the baric (on the left) and temperature (on the right) dependences of the function $\Delta_p = -(\partial \ln\sigma/\partial \ln\Sigma)_T$ of (5) along the said functions of the temperature and the pressure. As can be seen from the graphs, the function Δ_p varies linearly both with isothermal increase of the pressure and with isobaric increase of the temperature.

It can be seen in the Figures 3 and 6 that the baric dependences of the derivative of the isothermal elastic modulus with respect to the pressure: $B'(P) = (\partial B_T/\partial P)_T$, and of the derivative of the specific surface energy with respect to the pressure: $\sigma'(P)_T = (\partial\sigma/\partial P)_T$ are similar. Figure 7 shows the dependences of the calculated function $\sigma'(P)_T$ (in $10^{-3}\,\mathrm{J/(m^2\cdot GPa)}$) on the value of $B'(P)$. Figure 7, *a* shows these dependences calculated along the isotherms (from bottom to top) 300, 1000, 2000 K. Figure 7, *b* shows these dependences calculated along the isobars 0, 50, 100 GPa. It can be seen that the dependence of the function $\sigma'(P)_T$ on the value of $B'(P)$ is linear along all the isotherms and along the isobar 0 GPa. This makes it possible to evaluate the magnitude $\sigma'(P)_T$ by the value of $B'(P)$. However, along the isobars 50 and 100 GPa this dependence has a more complex form, as shown in the insert of Figure 7, *b*.

Using the function $\sigma(P, T)$, it is possible to evaluate dependences of the Poison's ratio μ_P on the pressure and the temperature. These dependences were calculated using the formula obtained in the Ref. [46] and tested in the Ref. [47]:

$$\mu_P(R, T) = \frac{1}{2} - \frac{1}{48 X_{sc}(R, T)[\gamma(R)]^2},$$

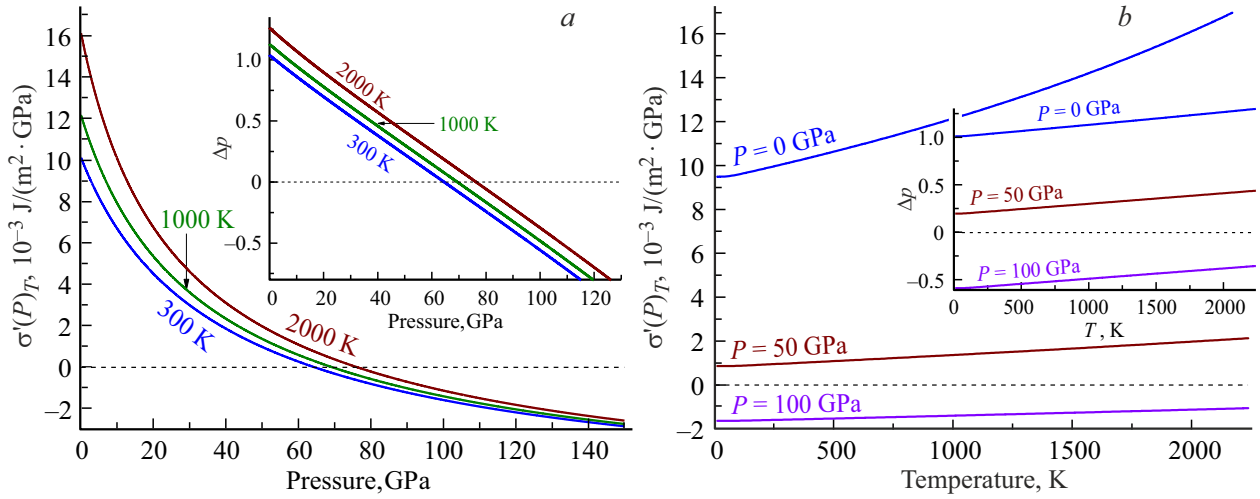


Figure 6. *a*) Baric and *b*) temperature dependences of the derivative of the specific surface energy with respect to the pressure. The inserts show the baric and temperature dependences of the function Δ_p. The baric dependences calculated along the isotherms 300, 1000, 2000 K. The temperature dependences calculated along the isobars 0, 50, 100 GPa.

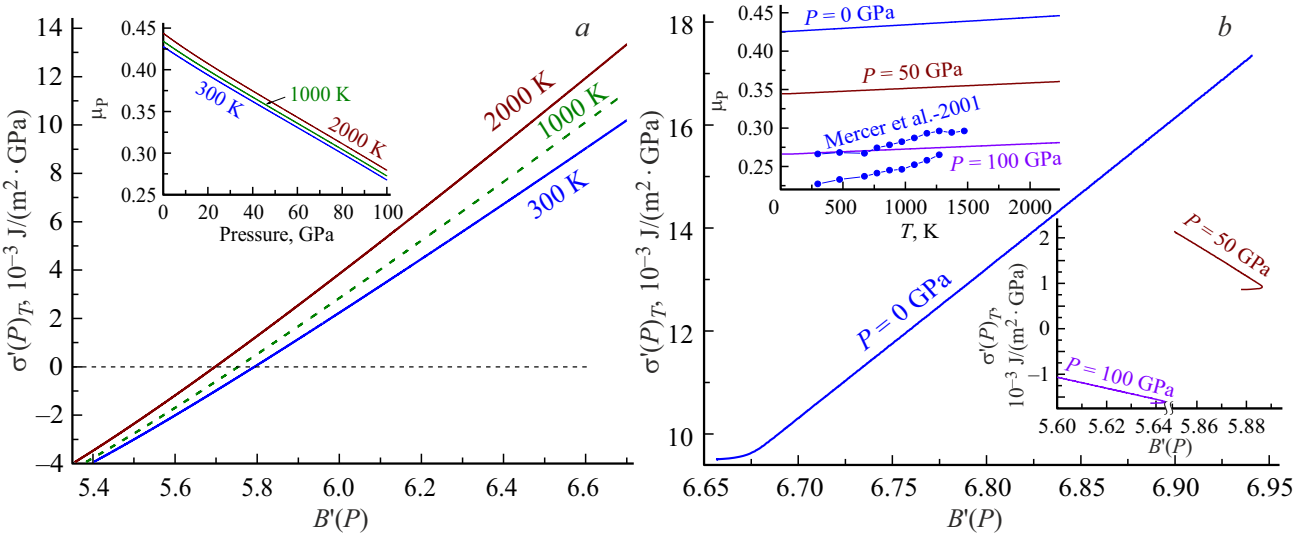


Figure 7. Dependences of the derivative of the specific surface energy with respect to the pressure on the derivative of the isothermal elastic modulus of FCC-Rh with respect to the pressure.*a*) Baric dependences calculated along the isotherms 300, 1000, 2000 K. The insert shows the baric dependence of the Poison's ratio.*b*) Temperature dependences calculated along the isobars 0, 50, 100 GPa. The insert shows the temperature dependence of the Poison's ratio.

wherein the function is introduced

$$X_{sc}(R, T) = \frac{\sigma(R, T)R}{r_0 B_T(R, T)}.$$

The inserts of Figure 7 shows the baric (Figure 7, *a*) and temperature (Figure 7, *b*) dependences μ_P. The temperature dependence μ_P for FCC-Rh when $P = 0$ was experimentally studied in the Ref. [48] by two different methods. The insert of Figure 7 shows results of the study [48] by solid circles. Our isobar, $P = 0$, lies somewhat higher than the values of the Ref. [48]. It can be seen from the inserts of Figure 7 that μ_P linearly decreases with isothermal increase of the pressure and linearly increases with isobaric increase of the temperature.

3.7. Melting point

Using the interatomic potential parameters from (8) and the method of the Ref. [25], the following values of the parameters of the formula (7) were obtained for FCC-Rh on the isotherm $T_m(0) = 2236$ K when $P = 0$.

$$c\left(0, T_m(0)\right) = 2.75269 \cdot 10^{-10}\,\text{m},$$

$$\Theta\left(0, T_m(0)\right) = 265.317\,\text{K}.$$

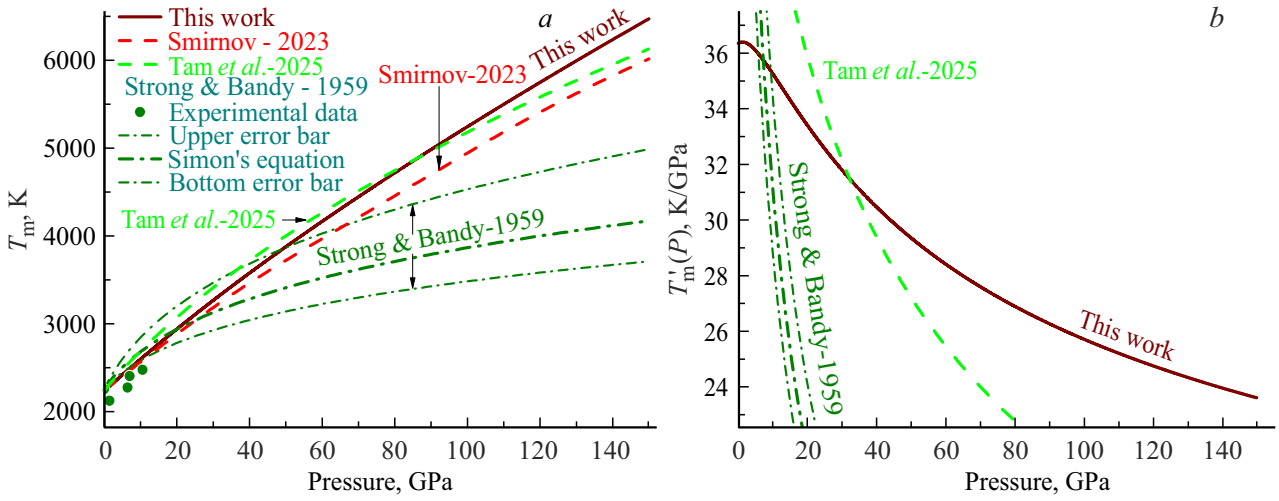


Figure 8. Baric dependence *a*) of the melting point *b*) and its derivative $T'_{\mathrm{m}}(P)$ with respect to the pressure for FCC-Rh. The solid line marks our results. The dashed lines show the results of calculations from the study [9] (lower) and the study [14] (upper). The dots of the left graph mark the results of the experiments from the study [1]. The dashdotted lines mark the dependence (11) of the study [1] and its upper and lower boundaries.

Figure 8, *a* shows the baric dependences for the melting point $T_{\mathrm{m}}(P)$ (in K), whereas Figure 8, *b* shows the baric dependences of the derivative of the melting point with respect to the pressure. $T'_{\mathrm{m}}(P) = dT_{\mathrm{m}}/dP$ (in K/GPa). The solid line marks our results. The function $T'_{\mathrm{m}}(P)$ was calculated by us by numerical differentiation of the dependence $T_{\mathrm{m}}(P)$ with respect to the pressure. The dashed lines show the results of calculations from the Ref. [9] (the lower line) and the Ref. [14] (the upper line). The dots of Figure 8, *a* show experimental results for FCC-Rh from the Ref. [1].

The function $T_{\mathrm{m}}(P)$ was approximated in the Ref. [1] by using the Simon–Glatzel equation of the following type:

$$T_{\mathrm{m}}(P) = T_{m0}\left[1 + \frac{P}{P_0}\right]^{c_s}. \qquad (11)$$

The following parameters $T_{m0} = 2253$ K, $P_0 = 7.22 \pm 0.7$ GPa, $c_s = 1/(5 \pm 1)$ were obtained for FCC-Rh in the Ref. [1]. This dependence is shown in Figure 8 by a thick dashdotted line. Thin dashdotted lines above and under it mark the upper (when $P_0 = 6.52$ GPa, $c_s = 1/4$) and the lower (when $P_0 = 7.92$ GPa, $c_s = 1/6$) boundaries of this dependence. In the Ref. [14], the results of calculations were FCC-Rh were also approximated by the Eq. (11) with the parameters $T_{m0} = 2236$ K, $P_0 = 21.8742$ GPa, $c_s = 0.4891$. In Figure 8, *a*, the dependence of the Ref. [14] is shown by a dashed line that lies above the calculations of the Ref. [9]. The right graph shows the derivative of the dependence (11) with respect to the pressure, which is calculated by the formula

$$T'_{\mathrm{m}}(P) = \frac{dT_{\mathrm{m}}(P)}{dP} = T_{m0}\,\frac{c_s}{P_0}\left[1 + \frac{P}{P_0}\right]^{c_s - 1}. \qquad (12)$$

In Figure 8, *b*, the functions $T'_{\mathrm{m}}(P)$ were calculated by the parameters provided in the Ref. [14]. It can be seen from Figure 8 that our results for FCC-Rh well agree with the results of the other authors.

3.8. Contribution by the electron subsystem to the baric dependences

As shown in the Ref. [11], at the high temperatures, when studying the FCC-Rh properties, it is also necessary to take into account a contribution by thermally-excited electrons. Then there is a question: how the baric and temperature dependences presented herein will be changed when taking into account the electron subsystem? When taking into account the electron subsystem, it is necessary to include the following summand into the specific free Helmholtz energy [49–51]:

$$f_{\mathrm{el}}(v, T) = -\frac{\chi_{\mathrm{el}}}{2N_A}\left(\frac{v}{v_0}\right)^{\gamma_{\mathrm{el}}} T^2, \qquad (13)$$

where N_A — the Avogadro's number, χ_{el} — the coefficient of electron heat capacity, which is determined from measurements of the heat capacity at the low temperature, γ_{el} — the electron Grüneisen parameter.

By assuming that the values of χ_{el} and γ_{el} do not depend on the temperature and the specific volume, it is easy to obtain expressions for additional contributions into the crystal properties from (13). For molar isochoric heat capacity, the equations of state and the isothermal elastic modulus, these contributions are written as follows

$$C_{v\,\mathrm{el}}(v, T) = \chi_{\mathrm{el}}\left(\frac{v}{v_0}\right)^{\gamma_{\mathrm{el}}} T, \qquad (14)$$

$$P_{\mathrm{el}}(v, T) = \gamma_{\mathrm{el}}\,\frac{\chi_{\mathrm{el}}}{2N_A v_0}\left(\frac{v}{v_0}\right)^{\gamma_{\mathrm{el}} - 1} T^2, \qquad (15)$$

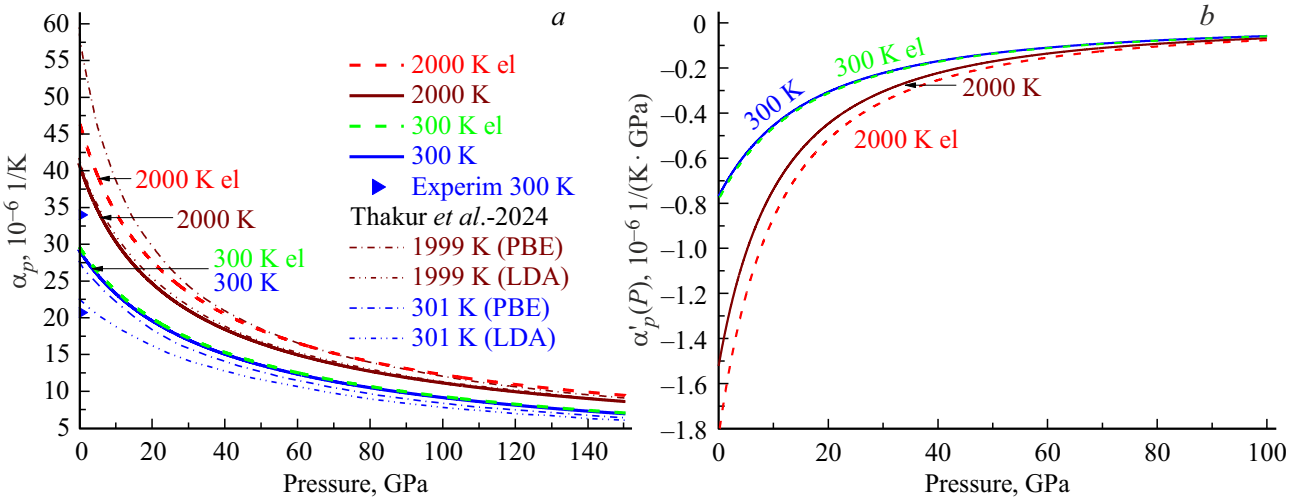


Figure 9. Baric dependence of *a*) the thermal expansion coefficient (the dashdotted lines — calculation of the isotherms 301 and 1999 K from the Ref. [11]: with one dot for the PBE method, with two dots — for the LDA method; the symbols of the vertical axis show results of the experimental studies at 300 K and when $P = 0$) and *b*) of the derivative of the thermal expansion coefficient with respect to the pressure for FCC-Rh. The solid lines mark our calculations at 300 and 2000 K without taking into account the electron subsystem. The dashed lines mark our calculations at 300 and 2000 K with taking into account the electron subsystem.

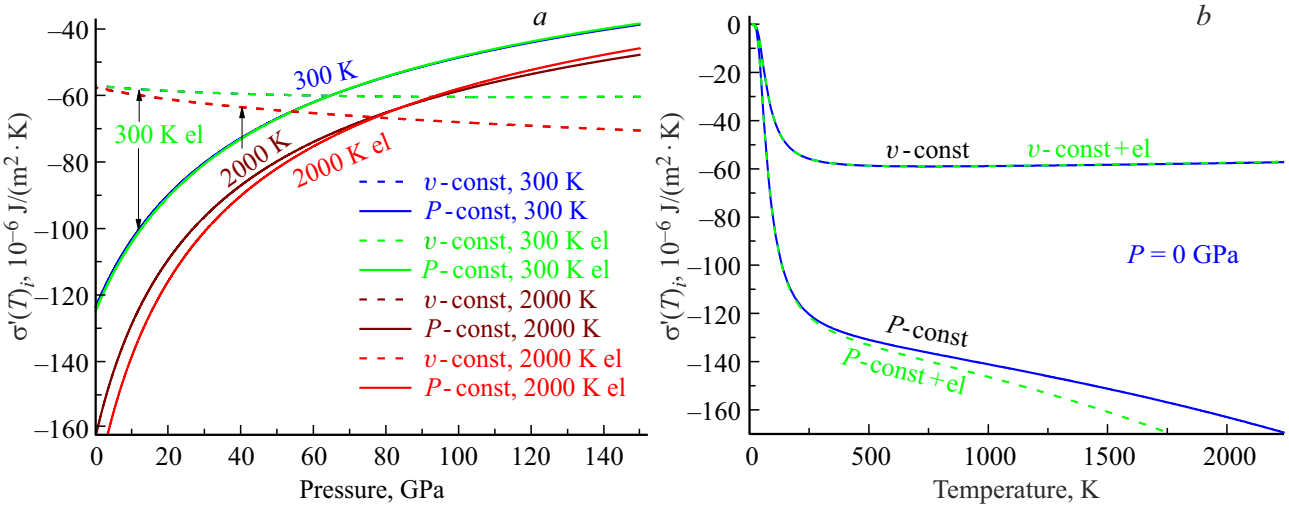


Figure 10. Dependences of the derivative of the specific surface energy of the facet (100) with respect to the temperature for FCC-Rh *a*) on the pressure and *b*) on the temperature. The baric dependences calculated along the isotherms 300 and 2000 K. The temperature dependences are calculated along the isobar $P = 0$ GPa. The solid lines mark the isobaric derivatives $\sigma'(T)_P$, while the dashed lines mark the isochoric derivatives $\sigma'(T)_v$.

$$B_{T\,\mathrm{el}}(v,T) = \gamma_{\mathrm{el}}(1-\gamma_{\mathrm{el}})\frac{\chi_{\mathrm{el}}}{2N_A v_0}\left(\frac{v}{v_0}\right)^{\gamma_{\mathrm{el}}-1} T^2. \qquad (16)$$

The expressions (14) and (16) can be used to obtain an expression for the volume thermal expansion coefficient as [52]

$$\alpha_{p\,\mathrm{el}}(v,T) = \gamma_{\mathrm{el}}\frac{C_{v\,\mathrm{el}}}{VB_T} = \gamma_{\mathrm{el}}\frac{\chi_{\mathrm{el}}}{N_A v_0 B_T}\left(\frac{v}{v_0}\right)^{\gamma_{\mathrm{el}}-1} T. \qquad (17)$$

Several methods were proposed to determine γ_{el}. For example, $\gamma_{\mathrm{el}} = 2/3$ is obtained [49–51] from the model of the perfect degenerate electron gas. $\gamma_{\mathrm{el}} = 1/2$ is followed [50,51] from the Thomas–Fermin model. The experimental estimates done at the low temperatures from the relationship [52]: $\gamma_{\mathrm{el}} = VB_T\alpha_{p\,\mathrm{el}}/C_{v\,\mathrm{el}}$, provided the following value for FCC-Rh: $\gamma_{\mathrm{el}}(\mathrm{Rh}) = 2.8 > \gamma(\mathrm{Rh})_{T=0\,\mathrm{K}} = 1.9$–$2.0$. However, it can be seen from the expression (16) that when $\gamma_{\mathrm{el}} > 1$, then $B_{T\,\mathrm{el}} < 0$, thereby indicating instability of this system. Therefore, in order to evaluate the contribution by the electron subsystem to the dependences of the FCC-Rh properties on the P–T-arguments we take that $\gamma_{\mathrm{el}} = 2/3$.

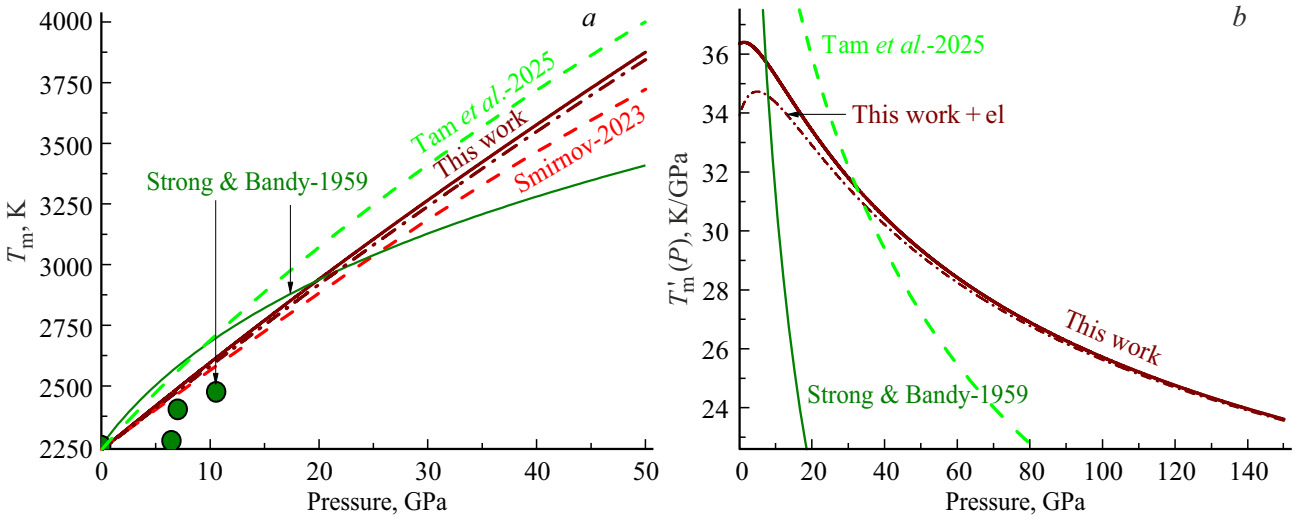


Figure 11. Baric dependence *a*) of the melting point T_m (the circles and the thin solid line mark the experimental results and the calculations according to the Eg. (11) of the Ref. [1]) and *b*) of its derivative $T'_m(P)$ with respect to the temperature for FCC-Rh. The solid line marks our results without taking into account the electron subsystem. The dashdotted lines show our results obtained taking into account the electron subsystem. The dashed lines show the results of calculations from the Ref. [9] (lower) and the Ref. [14] (upper).

The measurements of heat capacity at the low temperatures for FCC-Rh were taken to obtain [53] that $\chi_{el}(\mathrm{Rh}) = 4.65 \pm 0.018\,\mathrm{mJ/(mol \cdot K^2)}$. Hence,

$$\chi_{el}(\mathrm{Rh})T/(k_B N_A) = 0.56 \cdot 10^{-3}\,T. \qquad (18)$$

Using the method of the Refs. [15,16] taking into account the expressions (13)–(17) as well as using the potential parameters from (8) and the value from (18) and $\gamma_{el} = 2/3$, we have calculated the baric dependences of the FCC-Rh properties along the isotherms 300 and 2000 K.

The calculations have shown that of the studied dependences the following properties are negligibly changed: $P(T, v)$, $\Theta(T, P)$, $\gamma(T, P)$, $q(T, P)$, $z(T, P) = -(\partial \ln q/\partial \ln v)_T$, $B_T(T, P)$, $B'(P) = (\partial B_T/\partial P)_T$, $\sigma(T, P)$, $\sigma'(T)_v = (\partial\sigma/\partial T)_v$, $\sigma'(P) = (\partial\sigma/\partial P)_T$, Δ_p, μ_P. There is also no change of the dependence of the derivative of the specific surface energy with respect to the pressure on the derivative of the elastic modulus with respect to the pressure, which is shown in Figure 7. As shown in the Figures 9 and 10, the isotherm 2000 K has the following functions noticeably changed: $\alpha_p(T, P) = (\partial \ln v/\partial T)_P$, $\alpha'_p(P) = (\partial\alpha_p/\partial P)_T$, $\sigma'(T)_P = (\partial\sigma/\partial T)_P$. At the same time, as can be seen in Figure 9, *a*, the agreement of our dependence $\alpha_p(T = 2000\,\mathrm{K}, P)$ with the calculations of the Ref. [11] is improved. However, as can be seen from the Figures 9 and 10, with increase of the pressure along the isotherm 2000 K the contribution by the electron subsystem is reduced.

As can be seen from Figure 10, with taking into account the electron contribution, the dependence $\sigma'(T)_v$ is not changed, whereas the values of $|\sigma'(T)_P|$ somewhat increase at the low pressures and the high temperatures. With increase of the pressure, the influence of the electron subsystem is reduced. The baric dependence of the melting point has been calculated to show (Figure 11) that even at the low pressures the contribution by the electron subsystem is very small, and with increase of the pressure this contribution disappears.

4. Conclusion

Within the framework of the analytical method, the self-consistent method was used to calculate all the four parameters of the Mie–Lennard-Jones for FCC-Rh. The obtained potential parameters were used to calculate the Debye temperature, the Grüneisen parameter, the equation of state, the isothermal elastic modulus and the thermal expansion coefficient of FCC-Rh. It is shown that the calculated dependences well agree with the data that are obtained both experimentally and by means of computer simulation.

This is the first study that calculates for FCC-Rh the baric dependences of the derivatives of the isothermal elastic modulus: $B'(P) = (\partial B_T/\partial P)_T$ and the thermal expansion coefficient with respect to the pressure: $\alpha'_p(P) = (\partial\alpha_p/\partial P)_T$ along the isotherms 300, 1000, 2000 K. It was shown that the isotherms $B'(P)$ intersected each other in the point $P = 25\,\mathrm{GPa}$, $B'(P) = 6.13$. It indicates that at this pressure the function $B'(P)$ does not depend on the temperature.

It is for the first time that the FCC-Rh surface properties are calculated at the different P–T-conditions: the specific surface energy of the facet (100): $\sigma(100)$, its derivatives with respect to the temperature: $\sigma'(T)_i = (\partial\sigma/\partial T)_i$ (both the isochoric one: $i = v$, and the isobaric one: $i = P$) and the isothermal derivative of the function σ with respect to the pressure: $\sigma'(P)_T = (\partial\sigma/\partial P)_T$. We have obtained both the baric dependences of the said functions along the three

isotherms: 300, 1000, 2000 K as well as the temperature dependences along the three isobars: 0, 50, 100 GPa.

We have also obtained the estimates for the FCC-Rh fragmentation point at the various temperatures. It is shown that the function $\sigma'(P)_T$ for FCC-Rh linearly depends on the value of the isothermal derivative of the elastic modulus with respect to the pressure $B'(P)$. The obtained results for the functions $B_T(P, T)$ and $\sigma(P, T)$ were used to study for the first time the dependences of the Poison's ratio of FCC-Rh on the pressure and the temperature.

And the obtained dependences were used to calculate the baric dependences of the melting point and its derivative with respect to the pressure for FCC-Rh. The good agreement with the literature-known data is obtained.

The influence of the electron subsystem on the baric dependences of the studied FCC-Rh properties is studied. It is shown that of the studied dependences the following properties are insignificantly changed: $P(T, v)$, $\Theta(T, P)$, $\gamma(T, P)$, $q(T, P)$, $z(T, P) = -(\partial \ln q/\partial \ln v)_T$, $B_T(T, P)$, $B'(P) = (\partial B_T/\partial P)_T$, $\sigma(T, P)$, $\sigma'(T)_v = (\partial\sigma/\partial T)_v$, $\sigma'(P) = = (\partial\sigma/\partial P)_T$, Δ_p, the Poison's ratio μ_P. At the high temperatures, the following dependences are noticeably changed: $\alpha_p(T, P) = (\partial \ln v/\partial T)_P$, $\alpha'_p(P) = (\partial\alpha_p/\partial P)_T$, $\sigma'(T)_P = = (\partial\sigma/\partial T)_P$. However, with increase of the pressure along the isotherm the contribution by the electron subsystem is reduced. Even at the low pressures, the contribution by the electron subsystem to the baric dependence of the melting point of FCC-Rh is very small, and with increase of the pressure this contribution disappears.

Acknowledgments

The author wishes to thank S.P. Kramynin, K.N. Magomedov, Z.M. Surkhaeva and M.G. Yakh'yaev for fruitful discussions and their help.

Funding

The study was supported by grant №25-23-00001 from the Russian Science Foundation, https://rscf.ru/project/25-23-00001.

Conflict of interest

The author declares that he has no conflict of interest.

References

[1] H.M. Strong, F.P. Bundy. Phys. Rev. **115**, *2*, 278 (1959). https://doi.org/10.1103/PhysRev.115.278
[2] S. Marsh. LASL Shock Hugoniot Data, v. 5. University California Press, Berkeley (1980).
[3] E. Walker, J. Ashkenazi, M. Dacorogna. Phys. Rev. B **24**, *4*, 2254 (1981). https://doi.org/10.1103/physrevb.24.2254
[4] L.V. Al'tshuler, S.E. Brusnikin, E.A. Kuz'menkov. J. Appl. Mech. Tech. Phys. **28**, *1*, 129 (1987). https://doi.org/10.1007/BF00918785
[5] J.W. Arblaster. Platinum Metals Rev. **41**, *4*, 184 (1997). https://citeseerx.ist.psu.edu/document?repid=rep1&type=pdf&doi=f01e89265db07a7910e2f79b9d2fe85544ae5b56
[6] G. Pan, C. Hu, P. Zhou, F. Wang, Z. Zheng, B. Liang. J. Mater. Res. **29**, *12*, 1334 (2014). https://doi.org/10.1557/jmr.2014.141
[7] P. Kumar, N.K. Bhatt, P.R. Vyas, V.B. Gohel. Eur. Phys. J. B **89**, *10*, 219 (2016). https://doi.org/10.1140/epjb/e2016-70367-0
[8] K.V. Yusenko, S. Khandarkhaeva, T. Fedotenko, A. Pakhomova, S.A. Gromilov, L. Dubrovinsky, N. Dubrovinskaia. J. Alloys. Compd. **788**, 212 (2019). https://doi.org/10.1016/j.jallcom.2019.02.206
[9] N.A. Smirnov. J. Appl. Phys. **134**, *2*, 025901 (2023). https://doi.org/10.1063/5.0158737
[10] M. Frost, D. Smith, E.E. McBride, J.S. Smith, S.H. Glenzer. J. Appl. Phys. **134**, *3*, 035901 (2023). https://doi.org/10.1063/5.0161038
[11] B. Thakur, X. Gong, A. Dal Corso. AIP Adv. **14**, *4*, 045229 (2024). https://doi.org/10.1063/5.0203098
[12] J.D. McHardy, C.V. Storm, M.J. Duff, C.M. Lonsdale, G.A. Woolman, M.I. McMahon, N. Giordano, S.G. MacLeod. Phys. Rev. B **109**, *9*, 094113 (2024). https://doi.org/10.1103/PhysRevB.109.094113
[13] J.L. Rodrigo-Ramon, S. Anzellini, C. Cazorla, P. Botella, A. Garcia-Beamud, J. Sanchez-Martin, G. Garbarino, A.D. Rosa, S. Gallego-Parra, D. Errandonea. Sci. Rep. **14**, *1*, 26634 (2024). https://doi.org/10.1038/s41598-024-78006-0
[14] N.T. Tam, L.T. Lam, H.K. Hieu. Phys. Lett. A **547**, 130450 (2025). https://doi.org/10.1016/j.physleta.2025.130450
[15] M.N. Magomedov. Phys. Solid State **63**, *10*, 1465 (2021). https://doi.org/10.1134/S1063783421090250
[16] M.N. Magomedov. Phys. Solid State **64**, *7*, 765 (2022). https://doi.org/10.21883/PSS.2022.07.54579.319
[17] E.A. Moelwyn-Hughes. Physical Chemistry, Pergamon Press, London (1961). 1333 p.
[18] L.A. Girifalco. Statistical Physics of Materials. J. Wiley & Sons Ltd., New York (1973). 346 p.
[19] Y. Kraftmakher. Phys. Rep. **299**, *2–3*, 79 (1998). https://doi.org/10.1016/S0370-1573(97)00082-3
[20] M.N. Magomedov. Tech. Phys **68**, *2*, 209 (2023). https://doi.org/10.21883/TP.2023.02.55474.190-22
[21] M. Matsui. J. Phys: Conf. Ser. **215**, *1*, 012197 (2010). https://doi.org/10.1088/1742-6596/215/1/012197
[22] X. Huang, F. Li, Q. Zhou, Y. Meng, K.D. Litasov, X. Wang, B. Liu, T. Cui. Sci. Rep. **6**, 19923 (2016). https://doi.org/10.1038/srep19923
[23] A.M. Molodets, A.A. Golyshev, D.V. Shakhrai. JETP **124**, *3*, 469 (2017). https://doi.org/10.1134/S1063776117030049
[24] D.K. Belashchenko. Phys. — Uspekhi **63**, *12*, 1161 (2020). https://doi.org/10.3367/UFNe.2020.01.038761
[25] M.N. Magomedov. Phys. Solid State **65**, *5*, 708 (2023). https://doi.org/10.21883/PSS.2023.05.56040.46
[26] P. Janthon, S.(A) Luo, S.M. Kozlov, F. Viñes, J. Limtrakul, D.G. Truhlar, F. Illas. J. Chemical Theory. Comput. **10**, *9*, 3832 (2014). https://doi.org/10.1021/ct500532v
[27] J. Park, B.D. Yu, S. Hong. Current Appl. Phys. **15**, *8*, 885 (2015). https://doi.org/10.1016/j.cap.2015.03.028
[28] M.N. Magomedov. Solid State Commun. **397**, 115833 (2025). https://doi.org/10.1016/j.ssc.2025.115833
[29] D.K. Belashchenko. Russ. J. Phys. Chem. A **94**, *10*, 1971 (2020). https://doi.org/10.1134/S0036024420100064

[30] W.R. Tyson. Canadian Metallurgical Quarterly **14**, *4*, 307 (1975). https://doi.org/10.1179/000844375795049997
[31] W.R. Tyson, W.A. Miller. Surf. Sci. **62**, *1*, 267 (1977). https://doi.org/10.1016/0039-6028(77)90442-3
[32] M. Methfessel, D. Hennig, M. Scheffler. Phys. Rev. B **46**, *8*, 4816 (1992). https://doi.org/10.1103/PhysRevB.46.4816
[33] A. Eichler, J. Hafner, J. Furthmüller, G. Kresse. Surf. Sci. **346**, *1–3*, 300 (1996). https://doi.org/10.1016/0039-6028(95)00906-X
[34] J. Xie, M. Scheffler. Phys. Rev. B **57**, *8*, 4768 (1998). https://doi.org/10.1103/PhysRevB.57.4768
[35] I. Galanakis, N. Papanikolaou, P.H. Dederichs. Surf. Sci. **511**, *1–3*, 1 (2002). https://doi.org/10.1016/S0039-6028(02)01547-9
[36] Q. Jiang, H.M. Lu. Surf. Sci. Rep. **63**, *10*, 427 (2008). https://doi.org/10.1016/j.surfrep.2008.07.001
[37] F. Aqra, A. Ayyad. Appl. Surf. Sci. **257**, *15*, 6372 (2011). https://doi.org/10.1016/j.apsusc.2011.01.123
[38] J. Wang, S.Q. Wang. Surf. Sci. **630**, 216 (2014). https://doi.org/10.1016/j.susc.2014.08.017
[39] A. Patra, J.E. Bates, J. Sun, J.P. Perdew. Proceed. National Academy of Sci. **114**, *44*, E9188 (2017). https://doi.org/10.1073/pnas.1713320114
[40] J.-Y. Lee, M.P.J. Punkkinen, S. Schönecker, Z. Nabi, K. Kádas, V. Zólyomi, Y.M. Koo, Q.-M. Hu, R. Ahuja, B. Johansson, J. Kollár, L. Vitos, S.K. Kwon. Surf. Sci. **674**, 51 (2018). https://doi.org/10.1016/j.susc.2018.03.008
[41] A. Seoane, X.M. Bai. Surfaces. Interfaces **45**, 103841 (2024). https://doi.org/10.1016/j.surfin.2023.103841
[42] A.A. Oni-Ojo, E.O. Aiyohuyin. J. Nigerian Assoc. Math. Phys. **67**, *1*, 79 (2024). https://doi.org/10.60787/jnamp-v67i1-347
[43] S.N. Zhevnenko, I.S. Petrov, D. Scheiber, V.I. Razumovskiy. Acta Materialia **205**, 116565 (2021). https://doi.org/10.1016/j.actamat.2020.116565
[44] M.N. Magomedov. Phys. Solid State **67**, *2*, 428 (2025). https://doi.org/10.61011/PSS.2025.02.60685.318
[45] M.N. Magomedov. J. Surf. Investigation. X-ray, Synchrotron & Neutron Technique **6**, *1*, 86 (2012). https://doi.org/10.1134/S1027451012010132
[46] E.F. Pichugin. Izvestiya Vysshikh Uchebnykh Zavedenii: Fizika **6**, 77 (1962). (In Russ.)
[47] M.N. Magomedov. Phys. Solid State **62**, *12*, 2280 (2020). https://doi.org/10.1134/S1063783420120197
[48] J. Merker, D. Lupton, M. Töpfer, H. Knake. Platinum Metals Rev. **45**, *2*, 74 (2001).
[49] C. Kittel. Introduction to Solid State Physics. J. Wiley & Sons Ltd., NY (1976).
[50] V.N. Zharkov, V.A. Kalinin. Equations of State for Solids at High Pressures and Temperatures. Consultants Bureau, N.Y. (1971).
[51] I.V. Lomonosov, S.V. Fortova. High Temperature **55**, *4*, 585 (2017). https://doi.org/10.1134/S0018151X17040113
[52] G.K. White, A.T. Pawlowicz. J. Low Temperature Phys. **2**, *5/6*, 631 (1970). https://doi.org/10.1007/BF00628279
[53] G.T. Furukawa, M.L. Reilly, J.S. Gallagher. J. Phys. Chem. Ref. Data **3**, *1*, 163 (1974). https://doi.org/10.1063/1.3253137

Translated by M.Shevelev